网络出版时间:2026-02-11 14:35:39 网络出版地址:https://link.cnki.net/urlid/34.1065.R.20260506.1136.023

多模态MRI影像组学诺莫图区分HER-2阴性乳腺癌分子亚型

汪 群[1],潘红利[1],李小虎[1],余永强[1],颜蕴文[2],侯唯姝[1]
(安徽医科大学第一附属医院[1]医学影像科、[2]乳腺外科,合肥 230022)

摘要 **目的** 探讨基于多模态磁共振成像(MRI)影像组学诺莫图区分人表皮生长因子受体-2(HER-2)阴性乳腺癌分子亚型的价值。**方法** 回顾性分析进行多模态MRI检查并确诊的HER-2阴性乳腺癌患者190例,分为HER-2低表达(n=108)和HER-2 0表达(n=82)两个分子亚型组。将病例按照7∶3的比例随机分层采样划分为训练集133例和测试集57例。收集患者的临床和多模态MRI影像学特征,提取基于T2加权成像(T2WI)、扩散加权成像(DWI)和动态对比增强(DCE)-MRI的影像组学特征,分别构建临床影像模型、单模态影像组学模型、多模态影像组学模型和联合模型;联合多模态影像组学评分(radsocre)和临床影像特征绘制诺莫图,以构建可视化预测模型。采用曲线下面积(AUC)比较上述不同模型区分HER-2低表达与0表达亚型效能。**结果** HER-2低表达组的radscore与HER-2 0表达组相比,在训练集(P<0.000 1)和测试集(P<0.01)中差异均有统计学意义。多模态影像组学模型在训练集和测试集中的AUC分别为0.914和0.836,优于单模态影像组学模型。联合模型诺莫图表现出最佳诊断效能(训练集AUC:0.930;测试集AUC:0.865)。**结论** 联合radsocre和临床影像特征构建的诺莫图能够准确区分HER-2阴性乳腺癌中的低表达与0表达亚型。

关键词 多模态MRI;影像组学;乳腺癌;人表皮生长因子受体-2;诺莫图
中图分类号 R445.2
文献标志码 A **文章编号** 1000-1492(2026)04-0715-09
doi:10.19405/j.cnki.issn1000-1492.2026.04.016

人表皮生长因子受体-2(human epidermal growth factor receptor-2,HER-2)是乳腺癌诊疗的关键生物标志物,HER-2低表达与HER-2 0表达乳腺癌虽同属HER-2阴性乳腺癌的分子亚型,却在病理特征、治疗反应及预后上存在差异,精准区分二者对临床决策具有重要意义[1-4]。基于多模态磁共振成像(magnetic resonance imaging,MRI)的影像组学凭借非侵入性和高通量特征分析的优势,已广泛应用于乳腺癌检出、分子亚型预测和治疗敏感性评估等方面[5-8]。但区分HER-2阴性乳腺癌分子亚型的相关研究仍较少[9]。该研究以传统分子分型中的HER-2阴性乳腺癌患者为研究对象,开发了基于多模态MRI的影像组学模型、临床影像模型及联合模型,绘制诺莫图,以探讨多模态MRI影像组学诺莫图无创预测HER-2低表达和0表达亚型乳腺癌的价值。

2026-02-01 接收
基金项目:国家自然科学基金项目(编号:82371928);安徽医科大学校科研基金项目(编号:2021xkj134);安徽省转化医学研究院科研基金项目(编号:2023zhyx-C37)
作者简介:汪 群,女,硕士研究生;
侯唯姝,女,博士,主任医师,副教授,硕士生导师,通信作者,E-mail:biyuntian33@163.com

1 材料与方法

1.1 病例资料 回顾性收集2018年4月—2023年6月在安徽医科大学附属第一医院接受乳腺多模态MRI检查、病理资料完整的新确诊乳腺癌患者的资料。最终纳入HER-2阴性乳腺癌女性患者190例,年龄26~78(47±10)岁,分为HER-2低表达组(n=108)和HER-2 0表达组(n=82)。采用分层抽样法将患者按7∶3比例随机分成训练集(133例,HER-2低表达组79例,HER-2 0表达组54例)和测试集(57例,HER-2低表达组29例,HER-2 0表达组28例)。纳入标准:① 病理确诊为乳腺癌,免疫组织化学(immunohistochemistry, IHC)染色和荧光原位杂交(fluorescence in situ hybridization, FISH)符合HER-2低表达或0表达诊断标准;② 治疗前2周内行MRI检查,MRI资料完整。排除标准:① MRI图像质量差,影响图像分割;② 病变最大径<10 mm,部分容积效应影响图像分析。

1.2 病理分型标准 目前,HER-2状态的检测主要通过对手术或穿刺活检获取的组织样本进行IHC和FISH。依据美国临床肿瘤学会(ASCO)/美国病理学家协会(CAP)指南[10],HER-2 0表达定义为IHC 0;HER-2低表达定义为:① IHC+或② IHC++且

FISH检测无扩增。

1.3 临床特征、多模态MRI影像特征收集和模型建立

1.3.1 临床特征、多模态MRI影像特征收集 临床特征包括年龄、月经状态、乳腺癌家族史、病灶活动度、病灶质地、Ki67表达水平和腋窝淋巴结转移。多模态MRI影像特征由2名分别具有7、14年乳腺MRI诊断经验的诊断医师独立阅片，意见分歧时通过讨论达成共识。测量和记录的特征为：腺体类型（a：脂肪型；b：少量腺体型；c：不均匀致密型；d：极度致密型）、病灶位置、病灶数量、病灶形态、病灶体积、强化类型、时间-信号强度曲线（time-signal intensity curve，TIC）、T2加权成像（T2-weighted imaging，T2WI）信号特征、扩散加权成像（diffusion-weighted imaging，DWI）信号特征和相应的表观扩散系数（apparent diffusion coefficient，ADC）值。

1.3.2 特征筛选与模型建立 首先使用单因素Logistic分析筛选出鉴别HER-2低表达和HER-2 0表达亚型有统计学意义的特征，然后使用多因素Logistic回归分析进一步筛选独立预测因子，构建临床影像模型。

1.4 扫描方法 使用Philips 3.0T MR扫描仪和32通道相控阵体圈对患者进行乳腺MRI扫描。标准化MRI扫描序列包括：① 横轴位快速自旋回波序列（fast spin echo，FSE）T1加权成像（T1-weighted imaging，T1WI）：重复时间（repetition time，TR）480.0 ms，回波时间（echo time，TE）7.61 ms；② 横轴位翻转恢复序列（short tau inversion recovery，STIR）T2WI，TR 8 200.0 ms，TE 170.0 ms；③ 横轴位DWI：TR 7 000.0 ms，TE 80 ms，b值=800 ms和1 000 ms；上述序列层厚5.0 mm，层间距1.0 mm；④ 动态对比增强（dynamic contrast-enhanced，DCE）-T1WI：横轴位3D容积内插快速扰相梯度回波序列Vibrant：TR 3.6 ms，TE 2.1 ms，FOV 350 mm × 350 mm，层厚1.2 mm，层间距0 mm。采集1个时相蒙片之后，经高压注射器团注造影剂钆双胺注射液欧乃影（速率3 mL/s，剂量0.1 mmol/kg），然后分别于造影剂注射后第60、120、180、240、300和360 s进行数据采集，扫描时间共6 min 17 s。

1.5 影像组学分析 影像组学分析流程包括了图像分割、特征提取和筛选、模型构建和模型验证。

1.5.1 图像分割和特征提取 将轴位DCE-T1WI第1期、T2WI和DWI序列的DICOM数据导入3D-Slicer，沿肿瘤边缘逐层手动进行感兴趣区（region of interest，ROI）图像分割，生成三维感兴趣区（3D volume of interest，VOI）。多灶性病变选择最大病变进行图像分割。图像分割由上述2名医师手动完成。1个月后，从训练集中随机选择10%的病例重新进行图像分割，使用双因素随机组内相关系数（intraclass correlation coefficient，ICC）评估观察者间信度和复测信度，ICC定义为较差（<0.50）、中等（0.50~0.75）、良好（0.76~0.90）和优秀（0.91~1.00）。

使用内置PyRadiomics特征库的数坤科技平台（北京数坤网络科技有限公司）提取VOI图像的高通量特征。为防止对单个特征的依赖，对提取特征进行标准差标准化处理（Z-score）。

1.5.2 特征降维和模型构建 特征降维：经Spearman相关性分析，剔除相关性≥0.9的冗余特征；然后使用“Select K Best”算法保留F值在前50%的特征；最后使用最小绝对收缩和选择算子（least absolute shrinkage and selection operator，LASSO）筛选最佳特征集，采用5折交叉验证法充分优化模型。

通过影像组学特征及其系数计算影像组学评分（radscore）：radscore=截距+$\beta_i \times X_i$。β为系数，X为特征，i为序数。使用Logistic回归（LR）算法分别构建基于DWI、T2WI和DCE-MRI的单模态模型及多模态MRI模型。

1.6 统计学处理 使用SPSS 25.0进行统计分析。计数资料用例数（百分比）[n(%)]表示，定量数据用$M(Q_1,Q_3)$表示。使用单因素和多因素Logistic回归分析筛选独立预测因子。采用瀑布图反映队列中radscore值的分布和排序，小提琴图直观展示重要连续变量radscore在不同组别中的分布差异。采用受试者工作特征曲线下面积（area under the curve，AUC）评估各模型的区分效能，校准曲线检验模型的拟合度，决策曲线分析（decision curve analysis，DCA）计算不同概率阈值下的临床净效益。采用DeLong检验比较不同模型间预测性能的差异。P<0.05为差异有统计学意义。

2 结果

2.1 一般资料 训练集和测试集患者的临床特征和多模态MRI影像特征差异均无统计学意义。见表1。训练集中，HER-2低表达组和HER-2 0表达组患者的肿块质地（P=0.015）、病灶体积（P<0.001）、TIC曲线（P=0.014）差异有统计学意义；测试集中，

表1 训练集与测试集患者的一般资料分析[n(%), $M(Q_1,Q_3)$]

Tab. 1 Baseline characteristics of training and testing sets [n(%), $M(Q_1,Q_3)$]

Clinical and radiographic features	Training set (n=133)	Testing set (n=57)	P value
Age (years)	46.00 (39.00, 52.00)	48.00 (42.00, 50.00)	0.705
Menstrual status			0.793
Postmenopausal	51 (38.35)	20 (35.09)	
Premenopausal	82 (61.65)	37 (64.91)	
Breast cancer history			0.108
Yes	8 (6.02)	0 (0)	
No	125 (93.98)	57 (100.00)	
Lesion mobility			0.423
Freely	74 (55.64)	36 (63.16)	
Poor	59 (44.36)	21 (36.84)	
Lesion quality			0.238
Soft	22 (16.54)	5 (8.77)	
Stiff	111 (83.46)	52 (91.23)	
Ki67 (%)			1.000
>20	94 (70.68)	41 (71.93)	
≤20	39 (29.32)	16 (28.07)	
Axillary lymph node metastasis			0.776
Positive	63 (47.37)	29 (50.88)	
Negative	70 (52.63)	28 (49.12)	
Glandular density			0.545
a or b	28 (21.05)	15 (26.32)	
c or d	105 (78.95)	42 (73.68)	
Lesion location			0.217
Left-sided	73 (54.89)	25 (43.86)	
Right-side	60 (45.11)	32 (56.14)	
No. of lesions			0.572
Single	98 (73.68)	39 (68.42)	
Multiple	35 (26.32)	18 (31.58)	
Lesion shape			1.000
Nodular or mass	105 (78.95)	45 (78.95)	
Non-mass	28 (21.05)	12 (21.05)	
Enhancement pattern			0.890
Homogeneous	19 (14.29)	7 (12.28)	
Heterogeneous	114 (85.71)	50 (87.72)	
TIC type			0.737
Ⅰ	4 (3.01)	3 (5.26)	
Ⅱ	87 (65.41)	36 (63.16)	
Ⅲ	42 (31.58)	18 (31.58)	
The T2 signal of the lesion			0.764
Hypotintense	6 (4.51)	4 (7.02)	
Isoitense	40 (30.08)	16 (28.07)	
Hyperintense	87 (65.41)	37 (64.91)	
Lesion volume (mm^3)	7 903.90 (3 460.10, 18 117.80)	5 683.40 (3 055.33, 17 472.00)	0.225
ADC ($\times10^{-3}$, mm^2/s)	0.82 (0.73, 0.91)	0.86 (0.73, 0.91)	0.651

两组间病灶体积(P=0.004)差异有统计学意义,其余特征组间差异无统计学意义。见表2。

2.2 临床影像特征筛选和模型构建 通过单因素和多因素Logistic回归筛选出肿块质地(P=0.010)

表2 训练集与测试集HER-2 0表达与HER-2低表达患者临床及多模态MRI影像学特征比较[n(%), $M(Q_1, Q_3)$]

Tab. 2 Comparison of clinical and multimodal MRI features in patients with HER-2 zero expression and HER-2 low expression between training set and testing set [n(%), $M(Q_1, Q_3)$]

Clinical and radiographicfeatures	Training set			Testing set		
	HER-2 zero(n=54)	HER-2 low(n=79)	P value	HER-2 zero(n=28)	HER-2 low(n=29)	P value
Age(years)	46.00 (38.25, 50.00)	47.00(40.00, 53.50)	0.149	48.00(45.00, 50.00)	47.00(40.00, 49.25)	0.493
Menstrual status			0.467			0.708
Postmenopausal	19 (35.19)	34 (43.04)		10 (35.71)	8 (27.59)	
Premenopausal	35 (64.81)	45 (56.96)		18 (64.29)	21 (72.41)	
Breast cancer history			0.395			0.237
Yes	3 (5.56)	2 (2.53)		0 (0)	3(10.34)	
No	51 (94.44)	77 (97.47)		28(100.00)	26 (89.66)	
Lesion mobility			0.539			0.925
Freely	27 (50.00)	45 (56.96)		18 (64.29)	20 (68.97)	
Poor	27 (50.00)	34 (43.04)		10 (35.71)	9 (31.03)	
Lesion quality			0.015			0.504
Soft	12 (22.22)	5 (6.33)		6 (21.43)	4 (13.79)	
Stiff	42 (77.78)	74 (93.67)		22 (78.57)	25 (86.21)	
Ki67 (%)			0.332			0.234
>20	40 (74.07)	51 (64.56)		24 (85.71)	20 (68.97)	
≤20	14 (25.93)	28 (35.44)		4 (14.29)	9 (31.03)	
Axillary lymph node metastasis			0.497			0.506
Positive	28 (51.85)	35 (44.30)		16 (57.14)	13 (44.83)	
Negative	26 (48.15)	44 (55.70)		12 (42.86)	16 (55.17)	
Glandular density			0.356			0.601
a or b	14 (25.93)	14 (17.72)		6 (21.43)	9 (31.03)	
c or d	40 (74.07)	65 (82.28)		22 (78.57)	20 (68.97)	
Lesion location			0.969			0.349
Left-sided	27 (50.00)	41 (51.90)		17 (60.71)	13 (44.83)	
Right-side	27 (50.00)	38 (48.10)		11 (39.29)	16 (55.17)	
No. of lesions			0.085			0.130
Single	35 (64.81)	63 (79.75)		16 (57.14)	23 (79.31)	
Multiple	19 (35.19)	16 (20.25)		12 (42.86)	6 (20.69)	
Lesion shape			1.000			0.706
Nodular or mass	44 (81.48)	65 (82.28)		19 (67.86)	22 (75.86)	
Non-mass	10 (18.52)	14 (17.72)		9 (32.14)	7 (24.14)	
Enhancement pattern			0.147			1.000
Homogeneous	4 (7.41)	14 (17.72)		4 (14.29)	4 (13.79)	
Heterogeneous	50 (92.59)	65 (82.28)		24 (85.71)	25 (86.21)	
TIC type			0.014			0.674
Ⅰ	5 (9.26)	1 (1.27)		1 (3.57)	0 (0)	
Ⅱ	28 (51.85)	58 (73.42)		17 (60.71)	20 (68.97)	
Ⅲ	21 (38.89)	20 (25.32)		10 (35.71)	9 (31.03)	
The T2 signal of the lesion			0.365			0.386
Hypotintense	2 (3.70)	2 (2.53)		4 (14.29)	2 (6.90)	
Isoitense	21 (38.89)	22 (27.85)		8 (28.57)	5 (17.24)	
Hyperintense	31 (57.41)	55 (69.62)		16 (57.14)	22 (75.86)	
Lesion volume (mm^3)	11 408.70 (6 470.47, 38 204.85)	5 045.60 (2 532.65, 10 794.20)	<0.001	13 745.10 (5 373.75, 49 792.75)	4 840.00 (2 792.60, 14 875.00)	0.004
ADC ($\times10^{-3}$, mm^2/s)	0.81(0.66, 0.92)	0.85(0.76, 0.91)	0.208	0.80(0.70, 0.90)	0.86(0.77, 0.96)	0.318

和病灶体积(P<0.001)2个特征为预测HER-2表达状态的独立预测因素，基于上述特征构建临床影像模型。见表3。

2.3 单模态影像组学模型 基于T2WI、DWI和DCE单模态的影像组学模型在训练集预测HER-2表达状态的AUC值分别为0.784(灵敏度0.886，特异度0.537)、0.819(灵敏度0.848，特异度0.704)和0.834(灵敏度0.899，特异度0.667)；在测试集分别为0.777(灵敏度0.759，特异度0.714)、0.751(灵敏度0.966，特异度0.607)和0.794(灵敏度0.931，特异度0.607)。见图1。

2.4 多模态MRI影像组学特征提取和模型构建

2.4.1 特征提取 图像分割的观察者间信度ICC中位数为0.898(0.855，0.925)，具有显著的可靠性。从T2WI、DWI和DCE图像中共提取出了2 971个影像组学特征，经预处理、Spearman相关性分析、单变量筛选和Lasso回归，最终7个特征被纳入影像组学模型，包括DWI模态1个特征、T2WI模态3个特征、DCE模态3个特征，得分系数见表4。

2.4.2 多模态影像组学模型 联合T2WI、DWI和

表3 临床影像学特征的单变量和多变量Logistic回归分析

Tab. 3 Univariate and multivariate Logistic regression analysis of clinical and imaging characteristics

Clinical and radiographic features	Univariate analysis		Multivariate analysis	
	OR (95%*CI*)	*P* value	*OR* (95%*CI*)	*P* value
Age	1.028 (0.992–1.067)	0.133	–	–
Menstrual status	0.718 (0.348–1.460)	0.364	–	–
Breast cancer history	2.265 (0.363–17.640)	0.380	–	–
Lesion mobility	0.756 (0.376–1.514)	0.429	–	–
Lesion quality	4.229 (1.461–14.050)	0.011	4.560 (1.462–16.080)	0.010
Ki67	1.569 (0.739–3.432)	0.248	–	–
Axillary lymph node metastasis	1.354 (0.677–2.723)	0.392	–	–
Glandular density	1.625 (0.699–3.788)	0.257	–	–
Lesion location	0.927 (0.463–1.855)	0.830	–	–
No. of lesions	0.468 (0.212–1.021)	0.057	–	–
Lesion shape	1.625 (0.389–2.379)	0.257	–	–
Enhancement pattern	0.371 (0.101–1.109)	0.097	–	–
TIC type	0.822 (0.426–1.575)	0.554	–	–
The T2 signal of the lesion	1.564 (0.831–2.982)	0.167	–	–
Lesion volume(mm^3)	0.945 (0.914–0.973)	<0.001	0.944 (0.911–0.972)	<0.001
ADC ($\times10^{-3}$, mm^2/s)	1.692 (0.906–8.225)	0.372	–	–

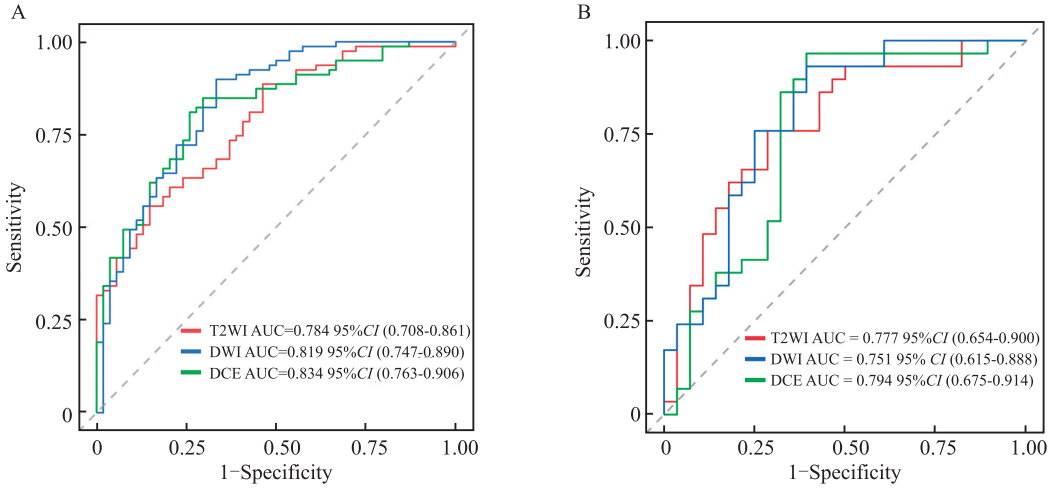

图1 基于T2WI、DWI及DCE-MRI的单模态影像组学模型鉴别训练集(A)和测试集(B) HER-2阴性乳腺癌亚型的ROC曲线图

Fig. 1 ROC curve of T2WI, DWI, and DCE-MRI based unimodal radiomics models for the identification of Training set (A) and Testing set (B) of HER-2 negative breast cancer subtypes

表4 多模态MRI影像组学特征提取

Tab. 4 Multimodal MRI radiomics feature extraction

Modality	Feature	Coefficient
DCE	Exponential_firstorder_Kurtosis	−0. 340 991 877
	Exponential_firstorder_Minimum	0. 617 847 415
	Gradient_firstorder_Variance	−0. 364 995 936
DWI	Log-sigma-3-0-mm-3D_glszm_SmallAreaEmphasis	−0. 164 593 498
	Wavelet-LHH_glszm_HighGrayLevelZoneEmphasis	0. 390 840 424
T2WI	Wavelet-LHL_glrlm_RunLengthNonUniformityNormalized	−0. 397 490 758
	Wavelet-LLH_glrlm_ShortRunHighGrayLevelEmphasis	0. 347 476 841

DCE序列的多模态MRI影像组学模型在训练集和测试集的AUC值分别为0. 914(灵敏度0. 924,特异度0. 815)和0. 836(灵敏度0. 759,特异度0. 821),诊断效能高于单模态模型(表5)。通过筛选的最佳影像组学特征及系数计算radscore,HER-2 0表达组和HER-2低表达组的radscore在训练集分别为−0. 910和0. 970,在测试集分别为−0. 980和0. 790。小提琴图显示HER-2低表达组的radscore与HER-2 0表达组相比,在训练集(P<0. 000 1)和测试集(P<0. 01)中差异均有统计学意义。见图2。

2.5 临床影像−影像组学联合模型及诺莫图构建

联合radscore和病灶体积、肿块质地构建临床影像−影像组学联合模型并绘制诺莫图,AUC值在训练集中为0. 930(灵敏度0. 911,特异度0. 852),在测试集为0. 865(灵敏度0. 966,特异度0. 697),均高于临床影像模型(训练集的AUC为0. 758,灵敏度为0. 633,特异度为0. 833;测试集的AUC为0. 722,灵敏度为0. 966,特异度为0. 464)和多模态MRI模型(表5和图3)。Delong检验显示,诺莫图预测HER-2表达状态的效能优于临床模型(P=0. 015),且其与多模态影像组学模型之间差异无统计学意义(P=0. 294)。校准曲线显示,3个模型对HER-2表达预测的准确度与实际情况有较好的一致性。DCA决

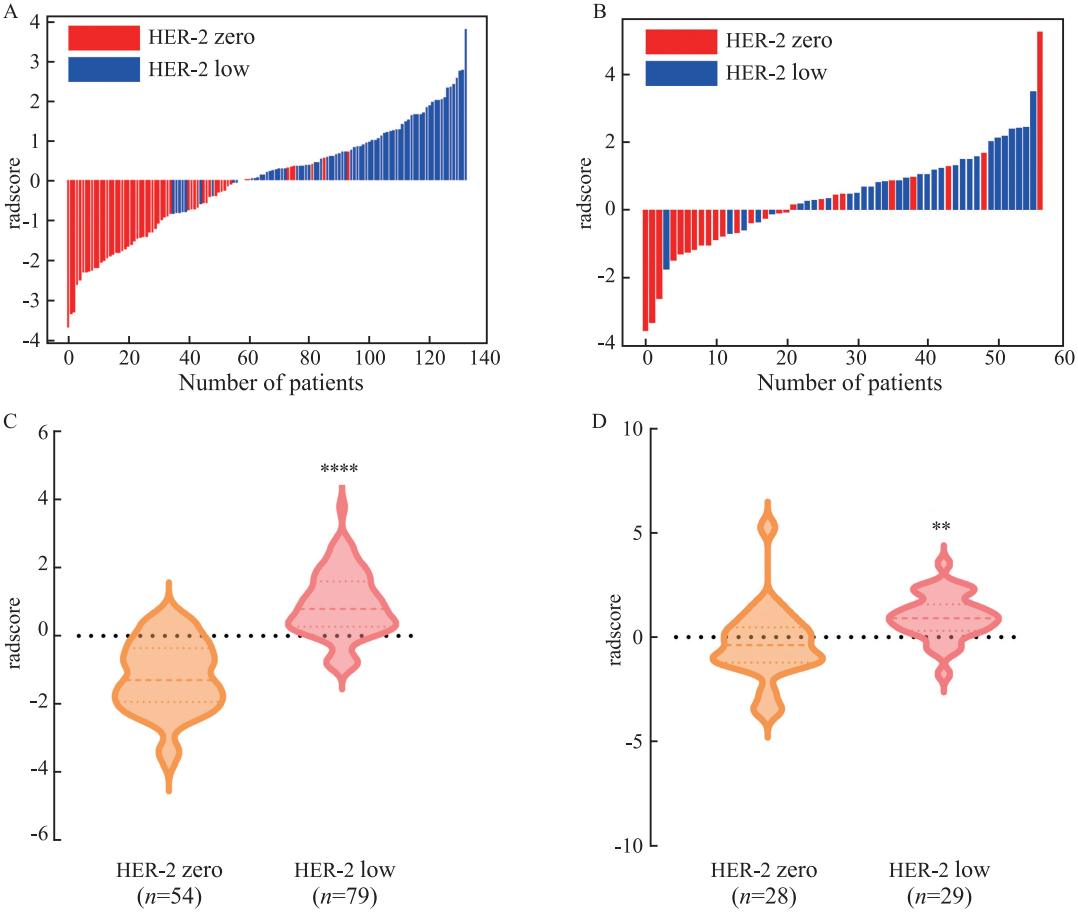

图2 影像组学分数区分HER-2阴性乳腺癌亚型

Fig. 2 Radscore differentiated HER-2-negative breast cancer subtypes

A: Training set waterfall plot; B: Testing set waterfall plot; C: Training set violin plot; D: Testing set violin plot; $^{**}P$<0. 01, $^{****}P$<0. 000 1 *vs* HER-2 zero group.

策曲线显示，诺莫图的临床净收益优于临床模型，当风险阈值为0.049~0.564、0.686~0.742时，临床净收益优于影像组学模型。见图3。

3 讨论

该研究联合多模态MRI影像组学和临床影像特征构建可视化诺莫图，用于预测HER-2阴性乳腺癌的分子亚型。研究表明，诺莫图能够准确区分HER-2低表达和HER-2 0表达亚型乳腺癌，radscore联合病灶体积、肿块质地等临床影像特征能够作为乳腺癌患者HER-2表达状态的重要预测指标。

在单模态MRI影像组学模型中，DCE-MRI影像组学模型表现出最佳的区分效能，这是由于DCE-MRI图像能够全面反映乳腺癌的形态和血流灌注信息，且较其他序列具有更高的空间分辨率和观察者间一致性[11]。T2WI在显示水肿、炎症等高水分含量的病变方面具有高敏感性，但作为单模态影像组学模型对HER-2表达状态的诊断效能较低，这与T2WI扫描时间短、层厚较厚和空间分辨率低等因素有关[12]。进一步的模型构建显示，多模态MRI影像

表5 各模型在训练集和测试集中预测HER-2阴性乳腺癌表达状态效能

Tab. 5 The performance of each model in predicting the expression status of HER-2 negative breast cancer in the training set and testing set

Model	Training set			Testing set		
	AUC (95%*CI*)	Sensitivity	Specificity	AUC (95%*CI*)	Sensitivity	Specificity
Clinical-radiological model	0.758 (0.674-0.842)	0.633	0.833	0.722 (0.580-0.855)	0.966	0.464
T2WI	0.784 (0.708-0.861)	0.886	0.537	0.777 (0.654-0.900)	0.759	0.714
DWI	0.819 (0.747-0.890)	0.848	0.704	0.751 (0.615-0.888)	0.966	0.607
DCE	0.763 (0.763-0.906)	0.899	0.667	0.794 (0.875-0.914)	0.931	0.607
Multimodal radiomics model	0.914 (0.860-0.968)	0.924	0.815	0.836 (0.735-0.938)	0.759	0.821
Combined model	0.930 (0.880-0.981)	0.911	0.852	0.865 (0.769-0.960)	0.966	0.697

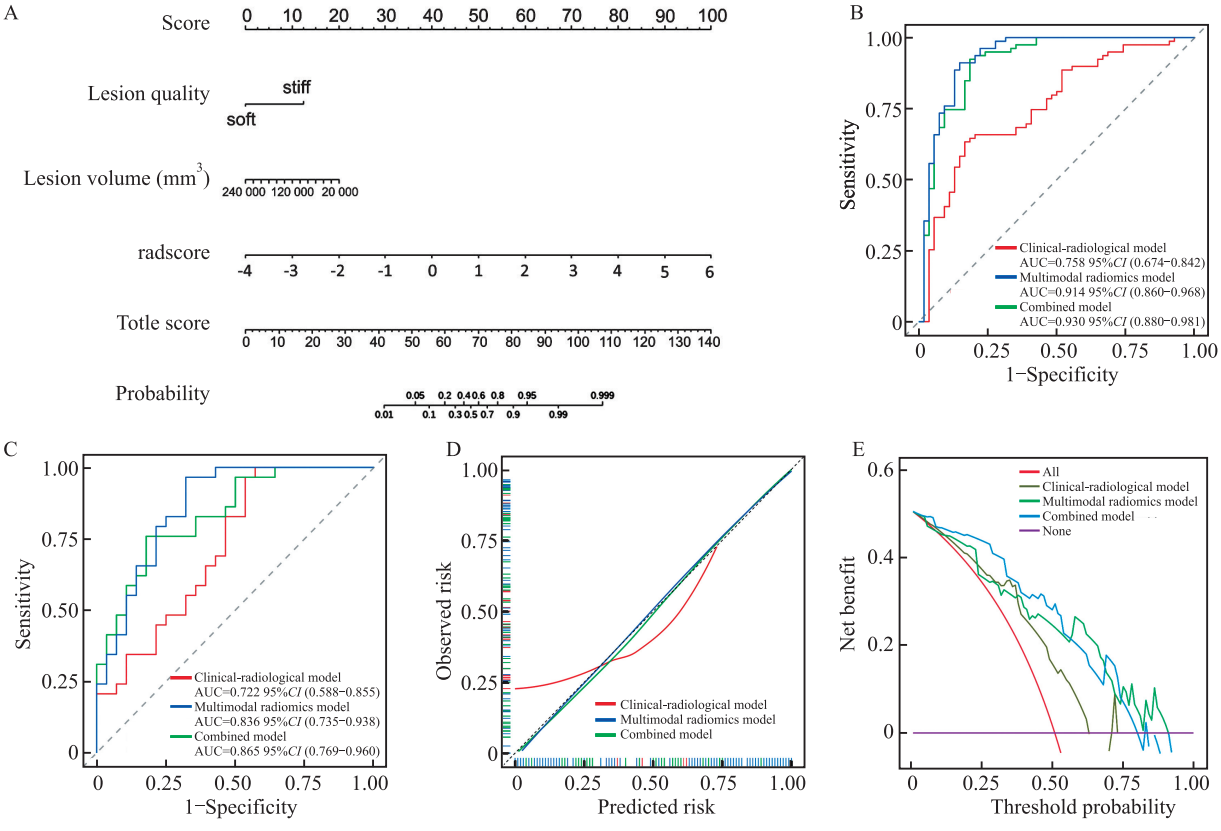

图3 不同模型区别HER-2阴性乳腺癌亚型的诺莫图(A)、训练集(B)和测试集(C)ROC曲线、校准曲线(D)和决策曲线(E)

Fig. 3 Nomogram (A), training set (B) and testing set (C) ROC curve, calibration curve (D) and decision curve (E) for different models to distinguish HER-2 negative breast cancer subtypes

组学模型诊断效能优于单模态MRI影像组学模型。多模态MRI能够反映肿瘤的形态、灰度、细胞增殖和微血管密度等多方面信息，充分展示了乳腺癌的高度异质性，具有显著的诊断优越性[13]。

小波特征是本研究基于T2WI提取的主要特征，具有多尺度分析的性能优势，能够同时捕获图像信号的多时域和多频域信息，从而揭示肉眼无法识别的乳腺癌组织的潜在异质性[14]。既往基于MRI的影像组学研究[15-16]已从多个角度验证了小波变换技术是乳腺癌影像特征提取中的关键作用，为本研究提供了理论支撑。从DCE-MRI图像提取的组学特征主要是一阶特征，映射肿瘤组织强化区域的分布和信号强度的变化，也是构建影像组学预测模型的重要因素。

本研究临床影像特征中，病灶体积是预测HER-2表达状态的独立预测因子，与Wu et al[17]和Yuan et al[18]的研究结果类似。HER-2过表达通过激活PI3K-AKT-mTOR通路增强细胞增殖与抗凋亡能力，从而驱动肿瘤生长，因此，HER-2低表达肿瘤可能体积更大[19]。然而训练集与测试集间肿块质地及TIC曲线表现不一致，可能与两组间病灶体积分布差异有关。训练集中若大病灶较多，其纹理和强化特征更突出，易使模型过拟合于此类非泛化特征，导致在测试集（病灶体积可能较小或分布不同）中判别效能下降。今后研究应考虑控制训练集与测试集的病灶体积匹配，以提高模型的泛化能力。本研究显示，诺莫图与多模态MRI影像组学模型均达到良好的诊断效能，但临床影像学特征的纳入进一步提升了诺莫图预测HER-2阴性乳腺癌分子亚型的AUC值，DCA也显示诺莫图展现出更高的临床净收益。

本研究存在一定局限性。作为单中心、回顾性研究，选择偏倚是其主要的局限性，需要多中心、前瞻性研究以进行验证模型的泛化性。此外，本研究使用手动分割病灶的方式，不可避免受到个人主观性的影响，未来将探讨半自动、自动的图像分割方式，使研究结果更加准确、客观。

参考文献

[1] Cortés J, Hurvitz S A, O'Shaughnessy J, et al. Randomized phase III study of amcenestrant plus palbociclib versus letrozole plus palbociclib in estrogen receptor-positive, human epidermal growth factor receptor 2-negative advanced breast cancer: primary results from AMEERA-5[J]. J Clin Oncol, 2024, 42(22): 2680-90. doi:10.1200/jco.23.02036.

[2] Hamilton E, Shastry M, Shiller S M, et al. Targeting HER2 heterogeneity in breast cancer[J]. Cancer Treat Rev, 2021, 100: 102286. doi:10.1016/j.ctrv.2021.102286.

[3] Mosele F, Deluche E, Lusque A, et al. Trastuzumab deruxtecan in metastatic breast cancer with variable HER2 expression: the phase 2 DAISY trial[J]. Nat Med, 2023, 29(8): 2110-20. doi:10.1038/s41591-023-02478-2.

[4] Vaz Batista M, Pérez-García J M, Cortez P, et al. Trastuzumab deruxtecan in patients with previously treated HER2-low advanced breast cancer and active brain metastases: the DEBBRAH trial[J]. ESMO Open, 2024, 9(9): 103699. doi:10.1016/j.esmoop.2024.103699.

[5] Luo L, Wu M, Li M, et al. A large model for non-invasive and personalized management of breast cancer from multiparametric MRI[J]. Nat Commun, 2025, 16(1): 3647. doi:10.1038/s41467-025-58798-z.

[6] Liu H, Chen X, Wang Y, et al. Background parenchymal enhancement in breast MRI correlates with molecular subtypes of breast cancer[J]. Curr Med Imaging, 2025: e15734056347327. doi:10.2174/0115734056347327250117073638.

[7] 赵 青，苏 桐，代 婷，等. 基于多参数MRI影像组学联合临床病理变量预测乳腺癌新辅助治疗的敏感性[J]. 磁共振成像，2024，15(6)：79-86. doi:10.12015/issn.1674-8034.2024.06.012.

[7] Zhao Q, Su T, Dai T, et al. Radiomics based on multiparametric MRI for prediction of breast cancers sensitive to neoadjuvant chemotherapy[J]. Chin J Magn Reson Imag, 2024, 15(6): 79-86. doi:10.12015/issn.1674-8034.2024.06.012.

[8] 陈剑琼，肖 榕，周玮珺，等. 灰阶超声影像组学在诊断乳腺结节良恶性中的应用价值[J]. 安徽医科大学学报，2022，57(2)：325-8. doi:10.19405/j.cnki.issn1000-1492.2022.02.031.

[8] Chen J Q, Xiao R, Zhou W J, et al. Ultrasound-based radiomics model in diagnosing benign and malignant breast nodules[J]. Acta Univ Med Anhui, 2022, 57(2): 325-8. doi:10.19405/j.cnki.issn1000-1492.2022.02.031.

[9] Zheng S, Yang Z, Du G, et al. Discrimination between HER2-overexpressing, -low-expressing, and-zero-expressing statuses in breast cancer using multiparametric MRI-based radiomics[J]. Eur Radiol, 2024, 34(9): 6132-44. doi:10.1007/s00330-024-10641-7.

[10] Wolff A C, Hammond M E H, Allison K H, et al. Human epidermal growth factor receptor 2 testing in breast cancer: American society of clinical oncology/college of American pathologists clinical practice guideline focused update[J]. J Clin Oncol, 2018, 36(20): 2105-22. doi:10.1200/jco.2018.77.8738.

[11] Lafcı O, Celepli P, Seher Öztekin P, et al. DCE-MRI radiomics analysis in differentiating luminal a and luminal B breast cancer molecular subtypes[J]. Acad Radiol, 2023, 30(1): 22-9. doi:10.1016/j.acra.2022.04.004.

[12] Zhang X, Teng X, Zhang J, et al. Enhancing pathological complete response prediction in breast cancer: the role of dynamic characterization of DCE-MRI and its association with tumor het-

erogeneity[J]. Breast Cancer Res, 2024, 26(1): 77. doi: 10.1186/s13058-024-01836-3.
[13] Zhang Z, Lan H, Zhao S. Analysis of the value of quantitative features in multimodal MRI images to construct a radio-omics model for breast cancer diagnosis[J]. Breast Cancer Targets Ther, 2024, 16: 305-18. doi:10.2147/BCTT.S458036.
[14] You C, Su G H, Zhang X, et al. Multicenter radio-multiomic analysis for predicting breast cancer outcome and unravelling imaging-biological connection[J]. NPJ Precis Oncol, 2024, 8(1): 193. doi:10.1038/s41698-024-00666-y.
[15] Sang L, Liu Z, Huang C, et al. Multiparametric MRI-based radiomics nomogram for predicting the hormone receptor status of HER2-positive breast cancer[J]. Clin Radiol, 2024, 79(1): 60-6. doi:10.1016/j.crad.2023.09.013.
[16] Yang Y, Wang J. Research on breast cancer pathological image classification method based on wavelet transform and YOLOv8[J]. J Xray Sci Technol, 2024, 32(3): 677-87. doi:10.3233/XST-230296.
[17] Wu J, Gong G, Cui Y, et al. Intratumor partitioning and texture analysis of dynamic contrast-enhanced (DCE)-MRI identifies relevant tumor subregions to predict pathological response of breast cancer to neoadjuvant chemotherapy[J]. J Magn Reson Imaging, 2016, 44(5): 1107-15. doi:10.1002/jmri.25279.
[18] Yuan C, Jin F, Guo X, et al. Correlation analysis of breast cancer DWI combined with DCE-MRI imaging features with molecular subtypes and prognostic factors[J]. J Med Syst, 2019, 43(4): 83. doi:10.1007/s10916-019-1197-5.
[19] Raghav K P S, Moasser M M. Molecular pathways and mechanisms of HER2 in cancer therapy[J]. Clin Cancer Res, 2023, 29(13): 2351-61. doi:10.1158/1078-0432.CCR-22-0283.

Nomogram based on multimodal MRI radiomics for discriminating molecular subtypes of HER-2-negative breast cancer

Wang Qun[1], Pan Hongli[1], Li Xiaohu[1], Yu Yongqiang[1], Yan Yunwen[2], Hou Weishu[1]
([1]*Dept of Medical Imaging*, [2]*Dept of Breast Surgery*, *The First Affiliated Hospital of Anhui Medical University*, *Hefei* 230022)

Abstract ***Objective*** To explore the value of a multimodal MRI-based radiomics nomogram for differentiating human epidermal growth factor receptor-2 (HER-2) negative breast cancer molecular subtypes. ***Methods*** A retrospective analysis was conducted on 190 patients with HER-2 negative breast cancer who underwent multimodal MRI examination, and the patients were divided into two molecular subtype groups: a HER-2 low expression group (n=108) and a HER-2 zero expression group (n=82). The cases were randomly stratified and sampled at a ratio of 7∶3 and divided into a training set of 133 cases and a testing set of 57 cases. The clinical and radiological features of the patients were collected, the radiomics features based on T2-weighted imaging (T2WI), diffusion-weighted imaging (DWI), and dynamic contrast-enhanced (DCE)-MRI were extracted, and the clinical-radiological model, unimodal radiomics model, multimodal radiomics model, and combined model were constructed respectively. Then the nomogram combined multimodal radiomics signature (radsocre) with clinical-radiological features was used to construct a visualized predictive model, and the area under the curve (AUC) was used to compare the effectiveness of different models in distinguishing HER-2 low expression and zero expression subtypes. ***Results*** A significant difference in radscore was demonstrated between the HER-2 low and HER-2 zero expression groups in both the training (P<0.000 1) and testing sets (P<0.01). The AUC of the multimodal radiomics model in the training set and the testing set were 0.914 and 0.836, respectively, which was superior to any unimodal radiomics model. The nomogram demonstrated great diagnostic efficacy (AUC=0.930 in training set; AUC=0.865 in testing set). ***Conclusion*** A multimodal MRI-based nomogram incorporating radsocre and clinical-radiological features can accurately distinguish the subtypes of HER-2 negative breast cancer.

Key words multimodal MRI; radiomics; breast cancer; human epidermal growth factor receptor-2; nomogram
Fund programs National Natural Science Foundation of China (No. 82371928); Scientific Research Project of Anhui Medical University (No. 2021xkj134); Research Project of Anhui Provincial Institute of Translational Medicine (No. 2023zhyx-C37)
Corresponding author Hou Weishu, E-mail: biyuntian33@163.com